Supplemental Material for "Shape-Dependent Friction Scaling Laws in Twisted Layered Material Interfaces"

Weidong Yan,[1#] Xiang Gao,[2#] Wengen Ouyang,[1,3,*] Ze Liu,[1,3,*] Oded Hod[2] and Michael Urbakh[2]

[1]*Department of Engineering Mechanics, School of Civil Engineering, Wuhan University, Wuhan, Hubei 430072, China*

[2]*School of Chemistry and The Sackler Center for Computational Molecular and Materials Science, Tel Aviv University, Tel Aviv 6997801, Israel*

[3]*State Key Laboratory of Water Resources Engineering and Management, Wuhan University, Wuhan, Hubei 430072, China*

#: These authors contribute equally to this work.

*Corresponding authors. Email: w.g.ouyang@whu.edu.cn, ze.liu@whu.edu.cn

This supporting information contains the following sections:

1. Static friction force definition

2. Effect of sliding direction

3. Effect of flexibility

4. Registry index calculations for twisted bilayer graphene

5. Scaling transition from polygonal to circular flakes

6. Irregular shaped flakes

7. Additional information on the analytical model for the static friction of graphene/*h*-BN polygonal contacts

8. A summary of scaling results

1 Static friction force definition

In the main text, we reported the contact size scaling of the static friction force for twisted rigid flakes of different shapes. Here, we show how we extract the sliding energy barriers and the corresponding static friction force from the sliding force traces of various flakes. In our atomistic calculation model (Fig. 1 in the main text), the top flake (graphene) is initially placed with its geometric center (appearing at the middle of its central hexagonal ring) located above one of the atoms of the underlying graphene or h-BN substrate. The flake is then shifted along the armchair direction of the corresponding substrate and the interlayer potential energy and the force acting on the flake are recorded.
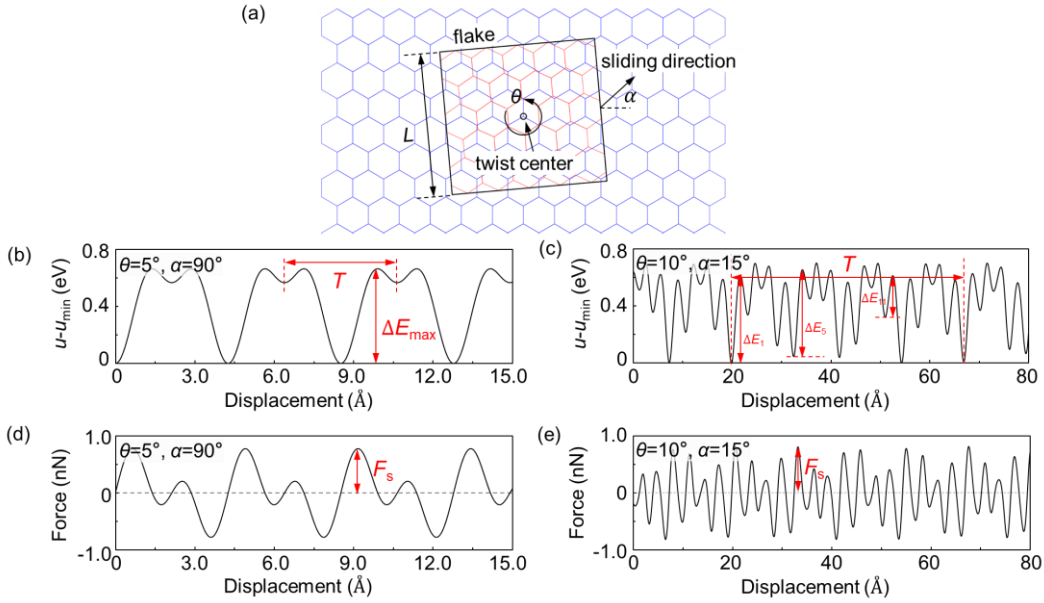
Fig. S1. The interlayer potential energy and corresponding resistive force experienced by a twisted square flake (of side length of $L = 14.5$ nm) along the scanline. (a) Schematic of the square flake model, where θ and α define the twist angle and sliding direction of the flake with respect to the zigzag direction of the substrate, respectively. Interlayer potential energy profiles (b, c) and the corresponding resistive force traces (d, e) are plotted for $\theta = 5°, \alpha = 90°$ (b, d) and $\theta = 10°, \alpha = 15°$ (c, e), respectively. Here, the resistive force is defined as the positive derivative of the potential energy trace along the sliding direction, corresponding to the external force required to move the slider. The maximal local potential energy barrier, sliding period, and the maximal resistive force are denoted by $\Delta E_{\max}$, T_s, and F_s, respectively.

For example, Fig. S1a illustrates a twisted square graphene flake, of twist angle θ and side length L, sliding along the α direction with respect to the zigzag axis of the substrate ($\alpha = 90°$ corresponds to

the chosen armchair sliding direction). And panels (b, c) show the atomistic calculation results of the interlayer potential energy as a function of sliding distance for such square flakes of side length L=14.5 nm and twist angle and sliding direction of (b) $\theta = 5°, \alpha = 90°$ and (c) $\theta = 10°, \alpha = 15°$. Panels (d) and (e) present the corresponding resistive force traces, where the static friction force (denoted by F_s) is defined as the maximal resistive force along the scanline period.

2 Effect of sliding direction

In the main text, we have presented results for various flakes sliding along the armchair direction of the substrate. To verify that this does not limit the generality of our conclusions, we compare in Fig. S2 the size dependence of the static friction force of $5°$ and $10°$ twisted square graphene flakes sliding along the armchair direction of the substrate $(\alpha = 90°)$ and the $\alpha = 15°$ direction. As long as the flake sides are not aligned with the moiré superlattice, the qualitative behavior of the size dependent static friction is found to be similar for both sliding directions considered, with some apparent quantitative differences.
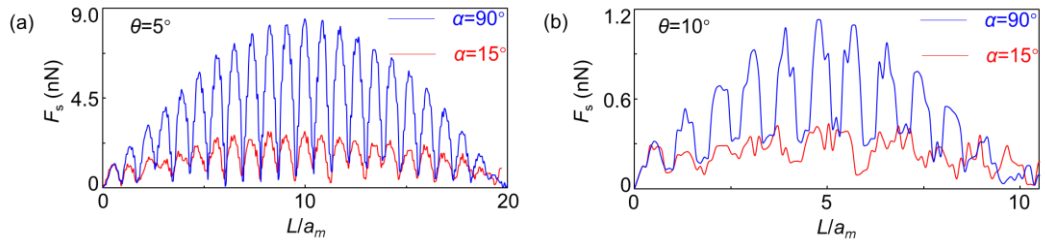
Fig. S2. Size dependence of the static friction force of square $5°$ (a) and $10°$ (b) twisted rigid graphene flakes sliding atop a fixed graphene substrate along the $\alpha = 90°$ (armchair, blue) and $\alpha = 15°$ (red) directions.

3 Effect of flexibility

In the main text we presented atomistic calculations performed using rigid flake model systems. This protocol neglects elasticity effects, which may influence friction. To evaluate the importance of such effect at the contact dimensions considered herein we refer to Ref. (Sharp et al., 2016), where it was suggested that a system can be considered as rigid when its dimensions are smaller than the characteristic length scale for elastic dislocations $b_{core} = (d \cdot G)/\tau_{max}$, where d is the lattice constant, G is the shear modulus, and τ_{max} is the maximum lateral shear stress experienced by an atom on the surface potential. To estimate b_{core} in our case, we consider the interlayer shear modulus of graphene $G = \sim 4.5$ GPa (Bosak et al., 2007; Shen et al., 2012), its lattice constant of $d = 2.46$ Å, and the shear stress of twisted bilayer graphene and twisted/aligned graphene/h-BN interfaces, which are of the order of $\tau_{max} = 0.01\text{-}0.1$ MPa (Koren et al., 2015; Song et al., 2018), yielding $b_{core} \approx$ 10-100 µm, which is 1-2 orders of magnitude larger than the typical dimensions considered in most relevant experiments. This indicates that elasticity effects are expected to kick-in only at the microscale and beyond.

As further verification of the rigid flake assumption, we performed dynamic friction calculations using flexible contact models. To this end, we constructed a six-layer graphene/h-BN system, where a three-layer graphene flake slides atop a three-layer h-BN substrate. The top flake layer is set to be rigid and moves along the armchair direction of the substrate with a constant velocity of 5 m/s. The bottom h-BN layer is kept rigidly fixed at its initial position. The zero-temperature and zero normal load dynamics of the atoms in all other layers is described using the REBO (Brenner et al., 2002) and Tersoff (Tersoff, 1988) intralayer and registry-dependent interlayer potentials (Leven et al., 2016b; Ouyang et al., 2018). To remove the heat generated during sliding, viscous damping with a damping coefficient of 1 ps^{-1} is applied to the middle flake layer and the middle h-BN layer, with minor effect on the dynamics of the shear interface. A similar simulation protocol was previously used successfully to describe the frictional properties of homogeneous and heterogeneous layered material interfaces (Gao et al., 2021a; Gao et al., 2021b).

First, to verify that our choice of sliding velocity provides converged results we compare in Fig. S3 the lateral force traces experienced by a 38.3×38.3 nm^2 graphene flake sliding on h-BN in the aligned configuration obtained with sliding velocities of 2 m/s and 5 m/s, as well as quasistatic simulation force traces representing the low velocity limit. For the latter, consecutive steps of displacing the top flake layer and optimizing the geometry using the FIRE algorithm (Bitzek et al., 2006; Guénolé et al., 2020), with a force convergence criterion of 2×10^{-4} eV/Å, have been performed. The results presented in Fig. S3 demonstrate that indeed a sliding velocity of 5 m/s provides well

converged results. Furthermore, the static friction values extracted from the dynamical simulations agree well with the result obtained from the rigid shift calculation.
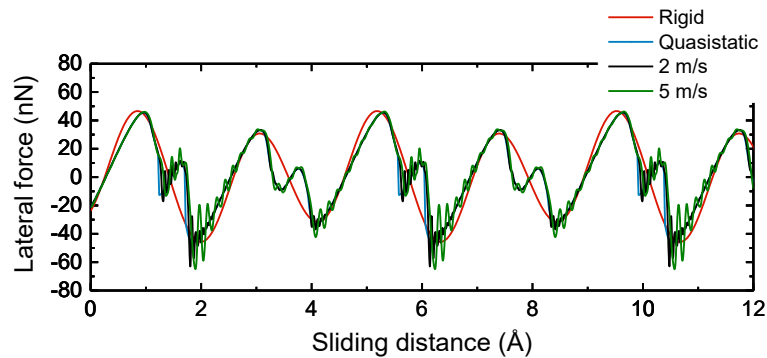
Fig. S3. Lateral force traces for a 38.3×38.3 nm^2 graphene flake sliding on h-BN in the aligned configuration obtained using the rigid flake model (red) and flexible flake models at different velocities (quasistatic – blue, 2 m/s black, and 5 m/s – green). The quasi-static trace corresponds to the low velocity limit.

Comparison of the size dependence of the static friction force obtained using rigid and flexible contact models appears in Fig. S4 for square shaped flakes in the aligned or 1° twisted configurations. For the aligned configuration (Fig. S4a), the static friction obtained via the flexible model simulations agrees well with the rigid calculations and the model predictions both in terms of the periodic variations and in terms of the size scaling of the upper envelope. Some small differences are found for the local minima, where the flexible simulations predict higher values that grow with contact size, mainly due to elasticity effects at the corners and edges of the square flakes, which results in imperfect compensation of incomplete moiré tiles along the edges. For the 1° twist square contact (Fig. S4b), the oscillatory behavior of static friction as a function of contact size is somewhat altered. For squares of sides smaller than ~ 50 nm the static friction force obtained in this case is up to twice as large as that of the rigid contacts. For larger flakes, the static friction force of the two protocols become comparable, where both do not exhibit any notable scaling with system size up to the largest contacts considered. These results thus justify the usage of rigid model calculations, which are highly computationally efficient, to study the static friction characteristics of large-scale layered interfaces.
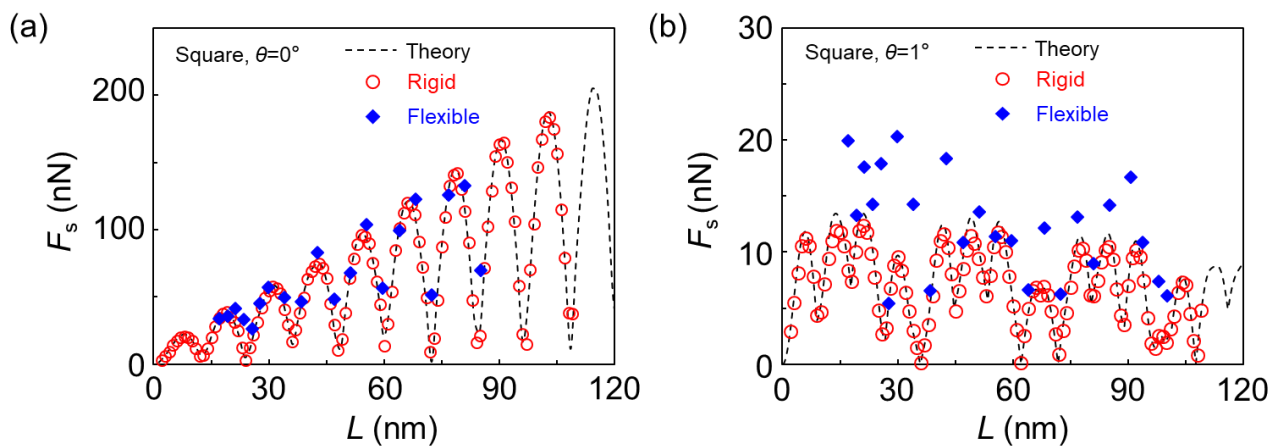
Fig. S4. Comparison of the size dependence of the static friction force obtained using rigid (red circles) and flexible (blue diamonds) square contact models sliding atop an *h*-BN substrate in (a) the aligned and (b) the 1° twisted configurations. Model predictions (Eqs. (A.7) and (A.11)) are shown by the black lines.

4 Registry index calculations for twisted bilayer graphene

The registry index is a simple geometric measure to evaluate the degree of commensurability between interfacing lattices (Hod, 2010), which effectively reflects the interlayer sliding potential of 2D materials (Hod, 2012). This measure is used in the main text to demonstrate the geometric origin of the double-periodicity in the static friction force dependence on contact size and the asymptotic scaling (or lack of).

To perform local registry index calculations (LRI) we adopted the protocol detailed in Ref. (Leven et al., 2016a), where the projected overlaps between circles placed around each atomic position in adjacent layers are averaged over the three nearest neighboring atoms to yield a local registry score. Since in the present study we focus on scaling laws with contact dimensions, the definition of the global registry index (GRI) had to be modified to account for the overall contact size as follows:

$$\text{GRI} = \frac{S(\theta)}{S_0(\theta)}, \tag{S4.1}$$

where $S(\theta) = \sum_{i=1}^{N} \sum_{j=1}^{M} S_{ij}$, S_{ij} is the projected overlap between the circles positioned around atom i in one layer and atom j in its adjacent layer, and the sum runs over all N atoms of the given layer and M atoms of its adjacent layer. The twist angle dependent normalization factor, $S_0(\theta)$, is the summation of circle overlaps over the area of one moiré superlattice. This normalization procedure, different than previous definitions (Hod, 2010), allows the registry index to encode also the size-scaling of the static friction force.

Fig. **S5** compares the interlayer potential (Ouyang et al., 2018) variation (black curve) of a 5° twisted square graphene flake of side length 1 nm rigidly sliding atop a fixed graphene surface and the corresponding GRI profile (red curve), showing good agreement between the two approaches.
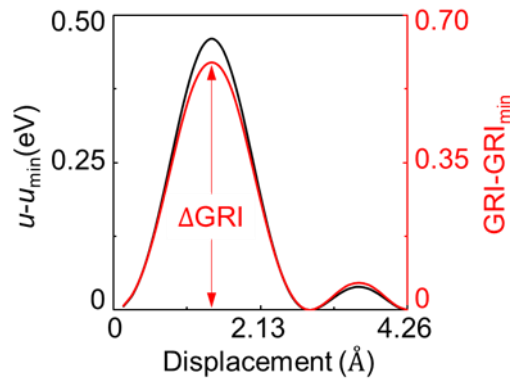
Fig. S5. Comparison between the interlayer potential variation (black curve) of a 5° twisted square graphene flake of side length of 1 nm, rigidly sliding atop a fixed graphene surface, and the corresponding GRI profile (red curve).

This demonstrates the intimate relation between the interlayer registry and the sliding potential energy landscape and allows for efficient evaluation of the interlayer energy for large interfaces. Fig. **S6** compares the size dependence of the sliding energy barrier obtained using atomistic calculations (black dashed lines) and the GRI approach (red circles), respectively, for different flake shapes and twist angles. In all cases considered, good agreement is obtained between the two approaches indicating the geometric origin of the double-periodic dependence of the static friction force on contact size and the asymptotic scaling (or lack of).
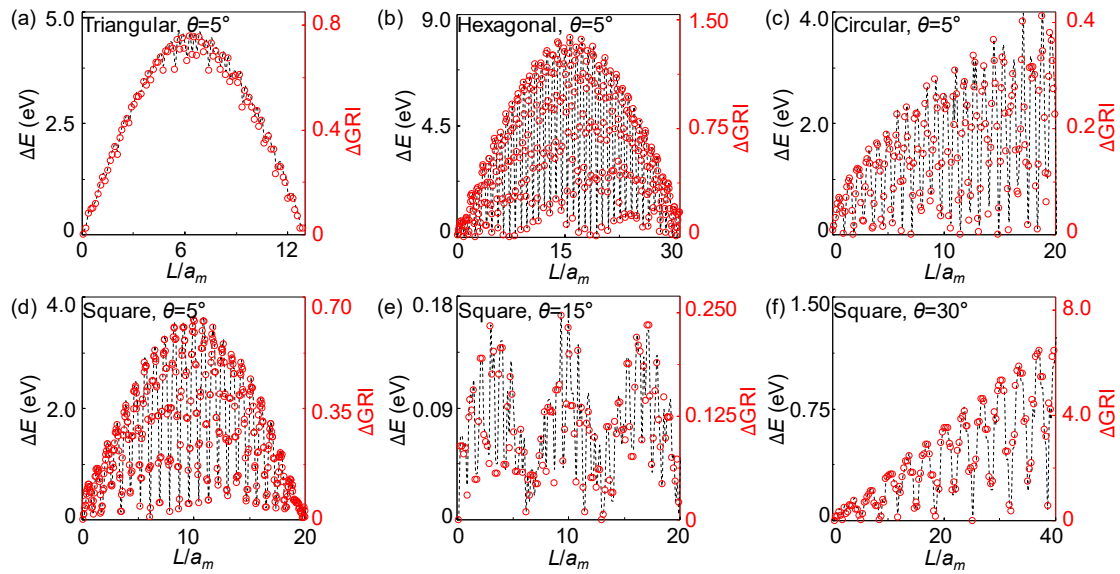
Fig. S6. Size dependence of the sliding potential energy barrier (black dashed lines) and the corresponding variations of the global registry index corrugation (ΔGRI, red circles) of graphene flakes of various shapes, rigidly sliding atop a fixed graphene surface with different twist angles. On the horizontal axes L is the side length (or circle radius) and a_m is the moiré superlattice period.

5   Scaling transition from polygonal to circular flakes

In the main text we have demonstrated that circular and polygonal flakes exhibit different scaling laws of the static friction with flake dimensions. Since a circular flake can be described as a polygonal flake in the limit of infinite number of sides, one would expect to obtain a smooth transition between the circular and polygonal flake scaling laws. To demonstrate this, we performed additional calculations for polygonal flakes with 12 and 50 sides twisted by 5° from the underlying lattice. For clarity, we plot the static friction force as a function of $\sqrt{A}$ (rather than L), where A is the surface area of the flake. As shown in Fig. S7, the long periodicity $\left(\sqrt{A_l}\right)$ of the static friction grows with increasing side number as $\sqrt{A_l} = \sqrt{\dfrac{N}{\tan(\pi/N)}}\dfrac{a_L}{2} \approx \dfrac{Na_L}{2\sqrt{\pi}}$, approaching infinity at the circular limit $(N \to \infty)$. This is manifested by the fact that the envelope of the $N = 50$ curve (blue) matches the curve of the circular flake (magenta).
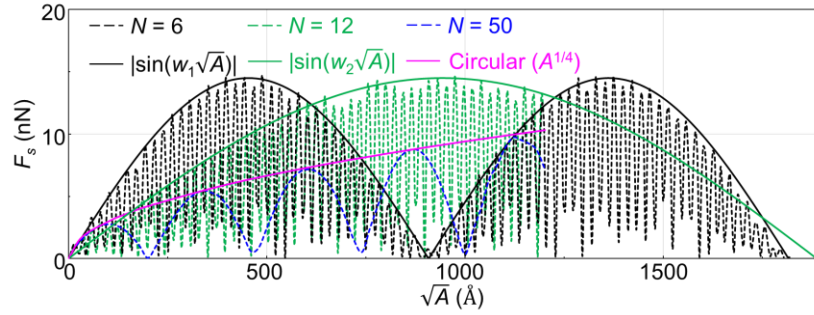
Fig. S7. Static friction scaling with the square root of the contact area for polygons of different number of sides $N = 6$ (black), 12 (green), and 50 (blue). The full lines mark the envelopes of the numerical solutions (dashed lines) obtained by numerical solution of the model presented in the main text. The analytical result obtained for the circular flake is presented in magenta.

6 Irregular shaped flakes

In the main text, the static friction forces of perfect polygonal or circular graphene flakes sliding atop a graphene or *h*-BN substrate are presented. These are rationalized by the compensation of incomplete moiré tiles along the flake sides. Questions arise whether the long-periodicity and absence of scaling with flake size associated with this effect prevail also in irregular shaped flakes, where efficient edge compensation of incomplete moiré tiles is jeopardized.

To answer these questions, we calculated the static friction force for four irregular-shaped 5° twisted rigid graphene flakes sliding on a fixed graphene substrate (see inset of Fig. S8 for the shape illustrations). Fig. S8 shows the static friction force dependence on contact size, demonstrating that the longer-period oscillations are manifested also for irregular shaped flakes that encompass either straight edges (Fig. S8a and c) or curved edges, the curvature of which does not vary with flake size (Fig. S8d). For the oval shaped flake (Fig. S8b) the double periodicity is much less pronounced, due to the variation of edge curvature with flake size, reminiscent of the case of circular flakes. Due to the less effective moiré tile compensation in curved flake sides, asymptotic increase of static friction with contact dimensions occurs when the edge curvature varies with flake size (see Fig. S8b and c), where a scaling exponent of ¼, similar to that observed for circular flakes, is found. We note that when the edge curvature approaches atomic spacing, the agreement between the continuum model and atomistic calculations results reduces (see Fig. S8e).
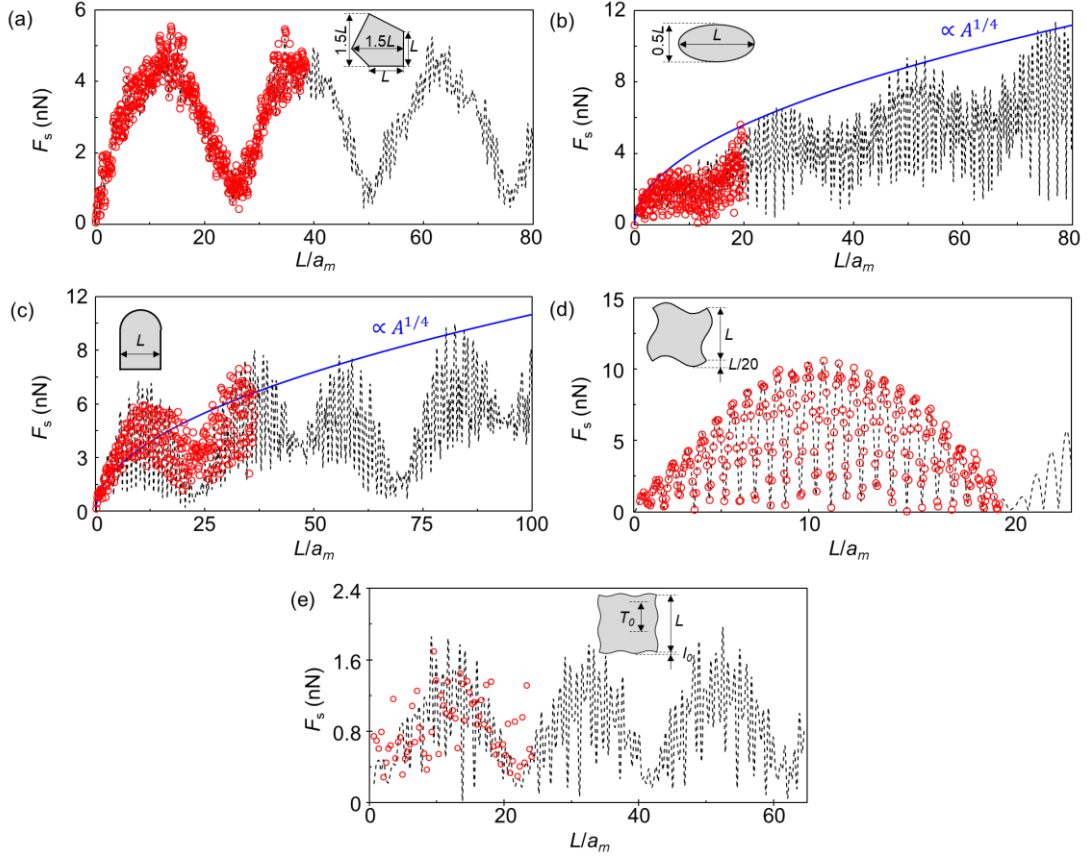
Fig. S8. Static friction force as a function of contact size for four irregular shaped rigid graphene flakes (see insets) sliding atop a fixed graphene substrate. Red circles and black dashed-lines represent atomistic calculation results and theoretical predictions, respectively. L, I_0 and T_0 are defined as depicted in the panel insets.

Another type of flakes, interpolating between equilateral square and circular flakes, are round-edged square flakes (see Fig. S9). In terms of edges, which are responsible for the complex frictional behavior discussed herein, these structures possess a combination of equilateral polygonal edges and perfect circular segments. The straight edges do not contribute to frictional scaling with edge size, due to the moiré tiles compensation effect. The circular sections, on the other hand, are expected to contribute to the scaling with an exponent of ¼. Nonetheless, since the four circular segments are shifted with respect to each other along the moiré superstructure, their contributions are not in phase, as in the case of a perfect circular flake so that the envelope behavior is less regular.
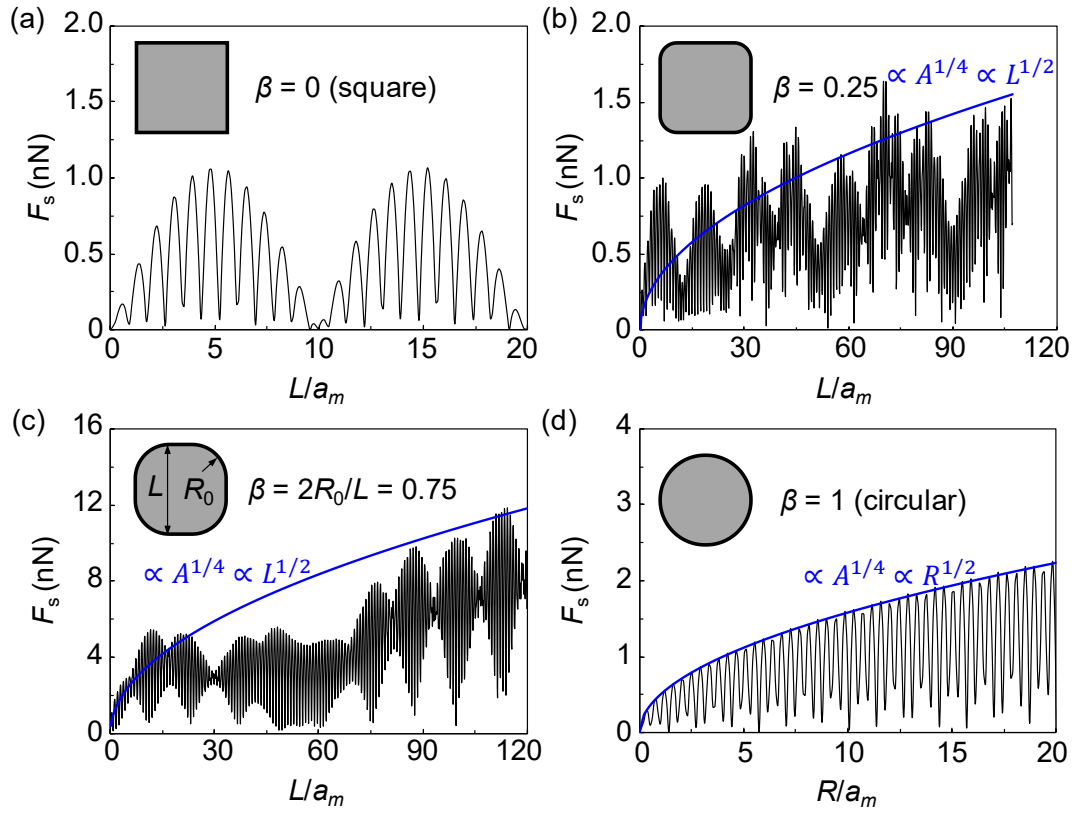
Fig. S9. Static friction force as a function of contact size for four rigid rounded-edged square graphene flakes. The circular fractions $\beta = 2R_0/L$ (see panel c) are (a) 0, (b) 0.25, (c) 0.75, and (d) 1, and the twist angle is chosen to be $\theta = 10°$.

7   Additional information on the analytical model for the static friction of graphene/*h*-BN polygonal contacts

The equations derived in the Appendix of the main text for the force experienced by generally twisted rigid polygonal graphene flakes as they slide atop a fixed *h*-BN surface have been used to derive simplified expressions for the case of aligned $(\theta = 0°)$ polygonal interfaces. This corresponds to the situation where the moiré superstructure is aligned with the side of the flake. The various angles appearing in the corresponding static friction expressions of graphene/*h*-BN polygonal contacts and the corresponding reference frames are shown in Fig. S10.
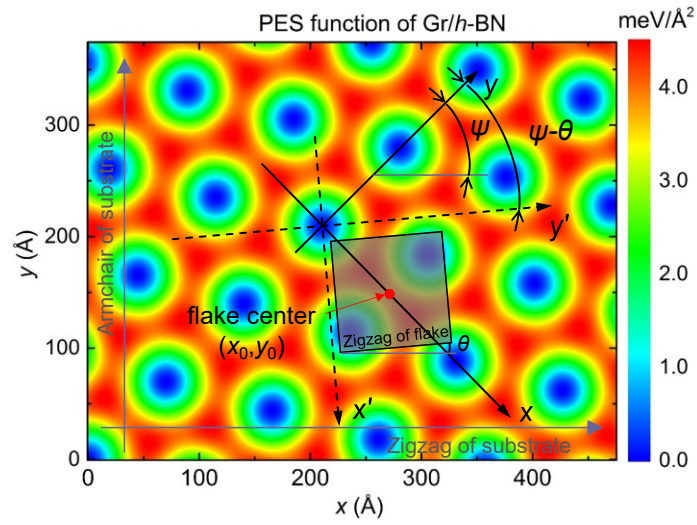
Fig. S10. Illustration of the moiré (x, y) and flake (x', y') reference frames plotted atop the potential energy density function (Eq. (4)) of a $\theta = 1°$ twisted square graphene flake sliding atop an *h*-BN surface. The reference frames are rotated with respect to each other by an angle of $\theta_1 = \psi - \theta = 43.9°$.

In fact, generally speaking, for polygonal shaped flakes with sides aligned with moiré superlattice directions, the static friction predicted by our model shows linear asymptotic scaling with the side length. The only exception we found is for square flakes sliding along the zigzag direction of the *h*-BN substrate, where no asymptotic growth is obtained and the static friction force reads as follows:

$$F_{s,sqr}(L) = \frac{8\sqrt{3}a_m^2 U_0}{9\pi a_{sub}} \left| \sin\left(\frac{\pi L}{\sqrt{3}a_m}\right) \sin\left(\frac{\pi L}{a_m}\right) \right|. \tag{7.1}$$

We note that for twisted heterojunctions, such as graphene/*h*-BN, due to the inherent lattice vectors mismatch the angle θ_1 strongly depends on the twist angle, θ, hence the approximations made to

obtain Eqs. (A.8) and (A.9) break already at very small twist angles $(\sim 1°)$ and one has to resort to the full expression of Eq. (A.7) of the Appendix of the main text to describe the size scaling of the static friction (see Fig. S11).
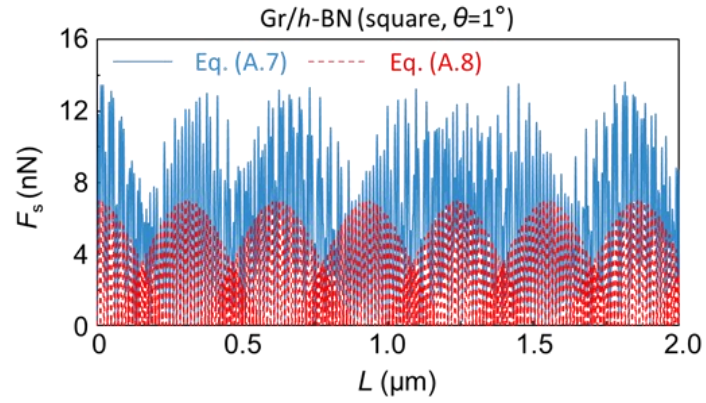
Fig. S11. Static friction force dependence on contact size for a 1° twisted square graphene flake rigidly sliding along the armchair direction of a fixed h-BN substrate. The blue line represents results obtained using the full expression of Eq. (A.7) and the red line shows the approximate results of Eq. (A.8).

8 A summary of scaling results

The following table summarizes the various scaling laws predicted for different flake shapes.

Table S1. Static friction scaling laws (A^γ) with respect to contact dimensions for different flake shapes

Flake shape	Potential energy surface	Scaling exponent
Circle		$\gamma = 0.25$
Hexagon		$\gamma = 0 \; (\theta_1 \neq 0)$ $\gamma = 0.5 \; (\theta_1 = 0)$ (Koren et al., 2016)
Square		$\gamma = 0 \; (\theta_1 \neq 0)$ $\gamma = 0.5 \; (\theta_1 = 0)$
Triangle		$\gamma = 0 \; (\theta_1 \neq 0)$ $\gamma = 0.5 \; (\theta_1 = 0)$
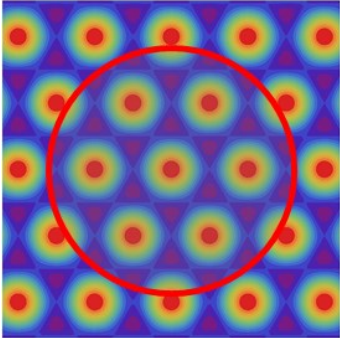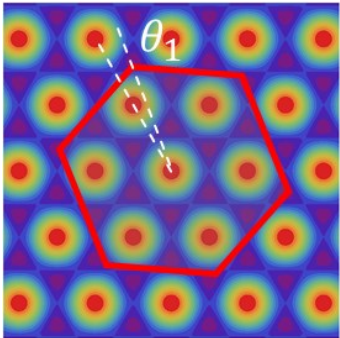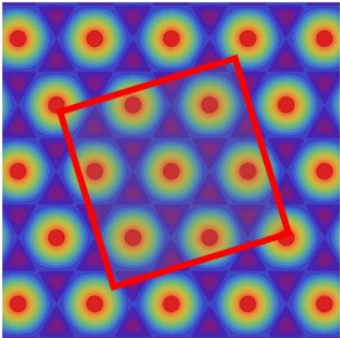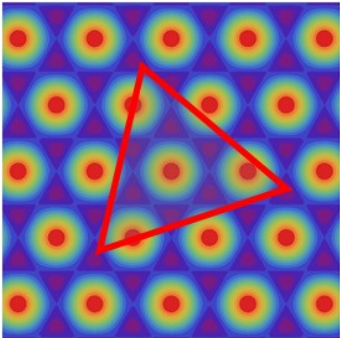
Irregular pentagon		$\gamma = 0 \;\; (\theta_1 \neq 0)$ $\gamma = 0.5 \;(\theta_1 = 0)$
Round-edged square		$\gamma = 0.25$
Ellipse		$\gamma = 0.25$
Window-shaped		$\gamma = 0.25$
Square with sinusoidal edges of fixed period and amplitude		$\gamma = 0$
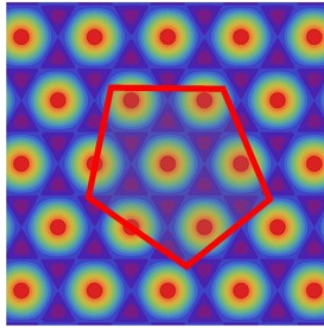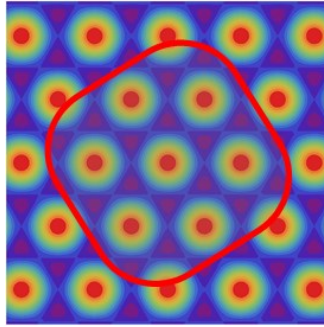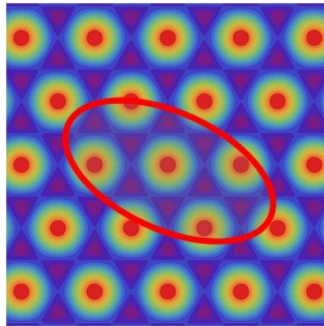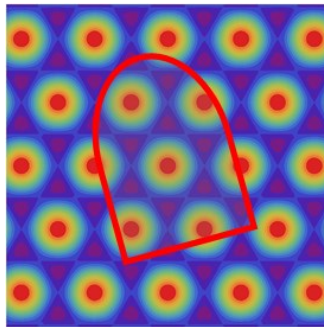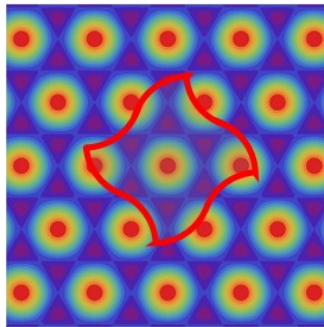
References

Bitzek, E., Koskinen, P., Gähler, F., Moseler, M. and Gumbsch, P. 2006. Structural Relaxation Made Simple. Phys. Rev. Lett., 97, 170201.

Bosak, A., Krisch, M., Mohr, M., Maultzsch, J. and Thomsen, C. 2007. Elasticity of Single-Crystalline Graphite: Inelastic X-ray Scattering Study. Phys. Rev. B, 75, 153408.

Brenner, D. W., Shenderova, O. A., Harrison, J. A., Stuart, S. J., Ni, B. and Sinnott, S. B. 2002. A second-generation reactive empirical bond order (REBO) potential energy expression for hydrocarbons. J. Phys.: Condens. Matter, 14, 783-802.

Gao, X., Ouyang, W., Hod, O. and Urbakh, M. 2021a. Mechanisms of frictional energy dissipation at graphene grain boundaries. Phys. Rev. B, 103, 045418.

Gao, X., Ouyang, W., Urbakh, M. and Hod, O. 2021b. Superlubric polycrystalline graphene interfaces. Nat. Commun., 12, 5694.

Guénolé, J., Nöhring, W. G., Vaid, A., Houllé, F., Xie, Z., Prakash, A. and Bitzek, E. 2020. Assessment and optimization of the fast inertial relaxation engine (fire) for energy minimization in atomistic simulations and its implementation in lammps. Comput. Mater. Sci, 175, 109584.

Hod, O. 2010. Quantifying the Stacking Registry Matching in Layered Materials. Israel J. Chem., 50, 506-514.

Hod, O. 2012. Interlayer commensurability and superlubricity in rigid layered materials. Phys. Rev. B, 86, 075444.

Koren, E. and Duerig, U. 2016. Moiré scaling of the sliding force in twisted bilayer graphene. Phys. Rev. B, 94, 045401.

Koren, E., Lörtscher, E., Rawlings, C., Knoll, A. W. and Duerig, U. 2015. Adhesion and friction in mesoscopic graphite contacts. Science, 348, 679-683.

Leven, I., Guerra, R., Vanossi, A., Tosatti, E. and Hod, O. 2016a. Multiwalled nanotube faceting unravelled. Nat. Nanotechnol., 11, 1082-1086.

Leven, I., Maaravi, T., Azuri, I., Kronik, L. and Hod, O. 2016b. Interlayer Potential for Graphene/h-BN Heterostructures. J. Chem. Theory Comput., 12, 2896-2905.

Ouyang, W., Mandelli, D., Urbakh, M. and Hod, O. 2018. Nanoserpents: Graphene Nanoribbons Motion on Two-Dimensional Hexagonal Materials. Nano Lett., 18, 6009.

Sharp, T. A., Pastewka, L. and Robbins, M. O. 2016. Elasticity limits structural superlubricity in large contacts. Phys. Rev. B, 93, 121402(R).

Shen, Y. and Wu, H. 2012. Interlayer shear effect on multilayer graphene subjected to bending. Appl. Phys. Lett., 100, 101909.

Song, Y., Mandelli, D., Hod, O., Urbakh, M., Ma, M. and Zheng, Q. 2018. Robust microscale superlubricity in graphite/hexagonal boron nitride layered heterojunctions. Nat. Mater., 17, 894-899.

Tersoff, J. 1988. New empirical approach for the structure and energy of covalent systems. Phys. Rev. B, 37, 6991-7000.